Journal of Industrial and Engineering Chemistry 117 (2023) 196–204

Contents lists available at ScienceDirect

Journal of Industrial and Engineering Chemistry

journal homepage: www.elsevier.com/locate/jiec

Synthesis of poly(3,4-ethylenedioxythuophene) derivatives using three-armed conjugated cross-linker and its thermoelectric properties

Jun Seop Lee [a], Shrayesh N. Patel [b,*]

[a] Department of Materials Science and Engineering, Gachon University, 1342 Seongnam-Daero, Sujeong-Gu, Seongnam-Si, Gyeonggi-Do 13120, Republic of Korea
[b] Pritzker School of Molecular Engineering, University of Chicago, 5640 South Ellis Avenue, Chicago, IL 60637, United States

ARTICLE INFO

Article history:
Received 8 July 2022
Revised 29 September 2022
Accepted 5 October 2022
Available online 13 October 2022

Keywords:
Organic thermoelectric
PEDOT
Electrical conductivity
Electrochemical polymerization
Co-polymer

ABSTRACT

Conducting polymer based thermoelectric systems are very effective at harvesting electricity from waste heat with low-temperature gradients relative to environmental temperature. However, although various studies concerning the doping effect exist, there are insufficient reports on the effect of the change in polymer chain structure on the thermoelectric properties. Here we demonstrate different poly(3,4-ethylene dioxythiophene) (PEDOT)-derivative chain structures (such as linear, two-dimensional, co-polymer), by varying the amount of three-armed conjugated cross-linker (1,3,5-tri(2-thienyl)-benzene (TTB)). At a small amount of TTB addition (until 0.5 mM), the electrochemical charge transport of the PEDOT films increased without shift of the UV–Vis absorbing property. However, from higher than 0.5 mM TTB, electrochemical charge transport decreased with blue shift of the UV–Vis absorbing curve. Moreover, the power factor of the PEDOT-derivative films without TTB to a small amount of TTB (0.5 mM) was improved from (27.03 to 49.43) μW m^{-1} K^{-2}, and at higher than 0.5 mM TTB concentration, was diminished, respectively, because a small amount of TTB enhanced the π–π interaction of the polymer chains without disrupting the conjugation, while excess TTB molecules blocked conjugation of the polymer.

Introduction

Conducting polymers for many organic electronics continue to attract interest, owing to their poly-conjugated chains that consist of single and double bonds [1–4]. Among various electronic applications, the conducting polymers are recently used as electrode materials for the thermoelectric generator. The thermoelectric generator is a secondary power system that generates electrical energy from industrial waste heat using the Seebeck effect [5–8]. The Seebeck effect is expressed using the Seebeck coefficient (S), which is a parameter that directly converts a temperature difference into an electrical voltage, and is a crucial index of the thermoelectric efficiency of material [9–11]. The effectiveness of the thermoelectric material is related to the dimensionless figure of merit (ZT), $ZT = S^2\sigma T/\kappa$, where S is the Seebeck coefficient, σ is the electrical conductivity, κ is the thermal conductivity, and T is the absolute temperature. In addition, the numerator of ZT ($S^2\sigma$) is defined as a power factor. From the definition of ZT, thermoelectric materials have to show large Seebeck coefficient (S) and electrical conductivity (σ) with low thermal conductivity (κ). In particular, the κ value of the conducting polymers that varies between (0.2 and 0.7) W m^{-1} K^{-1} from poly(3,4-ethylenedioxy thiophene) complexed with polystyrene sulfonic acid (PEDOT:PSS), to highly doped polyacetylene, is sufficiently small [12–14]. Therefore, many studies have worked to develop conducting polymers for high ZT with enhancing power factor.

Recent thermoelectric studies using conducting polymers, such as polycarbazole derivatives, display alluring characteristics with power factor of ca. 20 μW m^{-1} K^{-2} [15–17]. Poly(3,4-ethylenediox ythiophene) (PEDOT) is one of the most comprehensively investigated conducting polymers for electrode materials in thermoelectric application, because of its environmental stability, wide range of electrical conductivity, and solution processibility [18–20]. There are three possible approaches to modify the power factor of the PEDOT, which are control of the number of counter-ions, morphology, and microstructure of the polymer chains. First, controls of counter ion densities that balance the positive doping charge using polyanions (i.e., polystyrene sulfonate) and tosylate are the most common means to increase the power factor of the polymer [21–23]. In addition, tight molecular packing and strong intermolecular interaction between polymer layers using modified chain structure also increase the power factor [24,25]. However,

* Corresponding author.
E-mail address: shrayesh@uchicago.edu (S.N. Patel).

https://doi.org/10.1016/j.jiec.2022.10.004
1226-086X/

the studies of the power factor with different chain structures are inadequate.

2D planar pi-conjugated molecules have been used for the organic electronics due to their long-term stability and high charge-carrier mobility originating from the self-organized assemblies of chain structure [26–28]. In particular, star-shaped 2D pi-conjugated molecules have recently attracted interest as the active materials for organic electronics. The planarization of the star-shaped 2D conjugated system enhances parallel orientation to the substrate, and maximizes π-stacking interaction of the polymer chains. A number of star-shaped oligothiophene derivatives have previously been synthesized by Pepin-Donut et al. and Kotha et al. [29,30]. Additionally, to increase conjugation length of the polymer chain, branched oligothienylvinylenes were synthesized by the Roncali group [31]. Although high π-stacking and charge-carrier mobility have been reported for the latter crystals, no successful thermoelectric applications based on the star-shaped chain structure have so far been reported.

Herein, we report the synthesis of the PEDOT-derivative polymer chains through a facile electrochemical polymerization technique using a conjugated three-armed cross-linker (1,3,5-tri(2-thienyl)-benzene (TTB)). The structure of the polymer chains was modified with systematic change of TTB concentration, as follows: linear pristine PEDOT without TTB; two-dimensional PEDOT (2D PEDOT) for small amount TTB; copolymers of 3,4-ethylenedioxythiophene (EDOT) and TTB (PEDOT-co-TTB) for excess TTB; and polymerized TTB (poly-TTB) for only TTB addition (Fig. 1). The small amount of TTB addition enhanced electrochemical charge transport of the polymer films without shifting of the UV–Vis absorption, owing to TTB molecules enhancing π–π stacking in the structure, rather than interrupting conjugation of the chain. On the other hand, excess TTB molecules interrupted the conjugated chain structure with the formation of polymerized TTB in the polymer films. The thermoelectric properties of the as-prepared PEDOT derivatives were measured to implement thermoelectric application. The highest and lowest value of power factor were (49.43 and 0.84) μW m^{-1} K^{-2} at (0.5 and 3.0) mM TTB, respectively. The 2D chain structure enhances electrical conductivity by improving π–π stacking, and maintains a similar Seebeck effect to that of the polymer chains. To the best of our knowledge, no previous reports have described 2D PEDOT derivative chain structures and their use as electrode materials in thermoelectric application.

Materials and methods

Materials

3,4-Ethylenedioxythiophene (EDOT), 1,3,5-tri(2-thienyl)-benzene (TTB), tetrabutylammonium perchlorate, and propylene carbonate were purchased from Aldrich Chemical Co., and used without further purification.

Fabrication of PEDOT-derivative and poly-TTB films

Prior to synthesis, the ITO-coated PET film was cleaned with acetone, isopropanol (IPA), and distilled water, in sequence. The cleaned ITO-coated PET film was immersed in the electrolyte solutions that contained propylene carbonated as a solvent, 0.1 M tetrabutylammonium perchlorate as a salt, and 10 mM of EDOT and different concentration of (0.1–3.0) mM of TTB as monomers. PEDOT derivative films (thickness: *ca.* 1 μm) were produced *via* electro-polymerization using a three-electrode system consisting of the ITO-coated PET film as the working electrode, a platinum wire as the counter electrode, and an Ag/AgCl electrode as the reference electrode. The electro-polymerization was conducted at

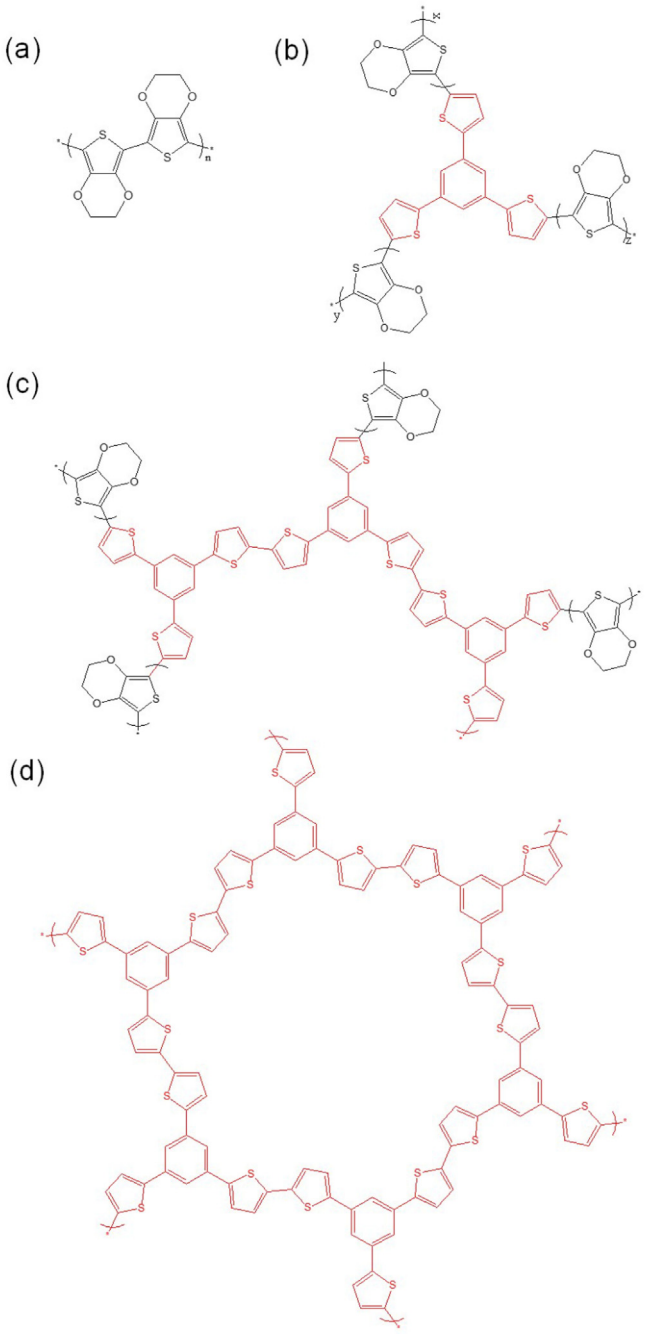

Fig. 1. Different structure of the polymer chains using 3,4-ethylenedioxythiophene (EDOT) and 1,3,5-tri(2-thienyl)-benzene (TTB) monomers: (a) pristine poly(3,4-ethylenedioxythiophene) (PEDOT), (b) two-dimensional PEDOT (2D_PEDOT), (c) co-polymers of EDOT and 1,3,5-tri(2-thienyl)-benzene (TTB) (PEDOT-co-TTB), and (d) polymerized TTB (poly-TTB).

RT over the voltage range of (−1.0 to +1.4) V (vs SEC) using 100 mV s^{-1} of scan rate for 10 cycles. Poly-TTB film was also synthesized using electrodeposition method from previous research paper [32]. After electro-deposition, the PEDOT-derivative decorated-PET films were removed, carefully washed with IPA, and dried at 60 °C for 2 h.

Characterizations

Hitachi S-2700 was used to obtained field-emission scanning electron microscopy (FE-SEM) images. Fourier-transform infrared

(FT–IR) and Raman spectra were measured using IRTracer-100 (Shimadzu) and LabRam HR Evo confocal Raman (Horiba, 785 nm), respectively. UV–Vis–NIR spectra were collected by UV-3600 Plus spectrophotometry (Shimadzu). X-ray photoelectron spectroscopy (XPS) was recorded using an Axis Nova (Kratos) with monochromatic Al–Kα X-ray source. Electrochemical impedance spectroscopy (EIS, frequency range: (1 MHz–1 Hz); amplitude: 20 mV) was conducted using an electrochemical workstation (Bio-logic SP-200). The internal structure of the PEDOT-derivative films was probed using Grazing Incidence Wide-Angle X-ray Scattering (GIWAXS). 2D GIWAXS images were obtained using beamline 8-ID-E at 432 station of the Argonne National Laboratory campus. The energy of the X-rays was 10.91 keV, the incidence angle (α) and the distance between sample and detector were set at 0.14° and 3 mm, respectively. The diffracted intensity was recorded by Pilatus CCD detector, and was normalized by the photon flux and acquisition time (10 s).

Thermoelectric coefficients measurement of the PEDOT-derivative films

To measure thermoelectric coefficients, PEDOT-derivative films were transferred from conductive substrate (ITO/PET) to insulating substrate (Epoxy/glass). In detail, insulating epoxy adhesive (Epoxies, #20-3302) coated glass substrate was placed on the PEDOT derivative film surface, and was cured at RT for 6 h. Then, the ITO/PET substrate was peeled away from the film surface to form the PEDOT/epoxy multilayers on the glass substrate. For the thermoelectric measurements, contacts were made to the samples after the transfer process using thermal evaporation of the gold through a shadow mask (Al). Electrical conductivity of films was measured using four-point probe measurement employing a Keithley 2400 source-meter unit and Keithley 6220 precision current source. Electrical conductivity (σ, S/cm) of the films was calculated using the following equation $\sigma = L/(R{\cdot}A)$, where L is the thickness of the film (cm), R is the resistance of the film (ohm), and A is the cross-sectional area of the film (cm^2) between the contacts. The thickness of the film (L) was measured using atomic force microscopy (AFM), and the resistance (R) was extracted from the slope of the VI steep using Ohm's law (V = IR). The Seebeck coefficient (S) measurements were performed using a custom-built set-up composed of two tungsten tips (Keithley 24000) to measure the voltage (V), and two thermocouple probes (Fluke 1529) to record the temperature (T). Peltier elements 5 mm apart provided the temperature difference ($\Delta T = T_H - T_C$). The measurement system has systematic error of 15 %, due to thermal anchoring issues. A delay of 100 s was used for voltage measurements to ensure that a steady-state temperature gradient was reached. The Seebeck coefficient was calculated from the slope of a linear fit for the ΔV vs ΔT plot. The measurements were taken within an approximate ΔT of ± 3 K around 300 K.

Results and discussion

Fabrication of PEDOT-derivative films

Different structure polymer chains from (3,4-ethylenedioxythiophene) (EDOT) and (1,3,5-tri(2-thienyl)-benzene (TTB) monomers were synthesized using electrochemical polymerization process (Fig. S1). The cleaned ITO/PET film was immersed in the electrochemical cell that contained different amount of monomers (EDOT and TTB) with propylene carbonate. The ITO/PET containing cell was subjected to cycle voltammetry (CV) scanning in the optimized potential range (−1 to +1.4) V with a three-electrode configuration of ITO/PET as the working electrode, Ag/AgCl as the reference electrode, and Pt wire as the counter electrode. In particular, the synthesized potential range

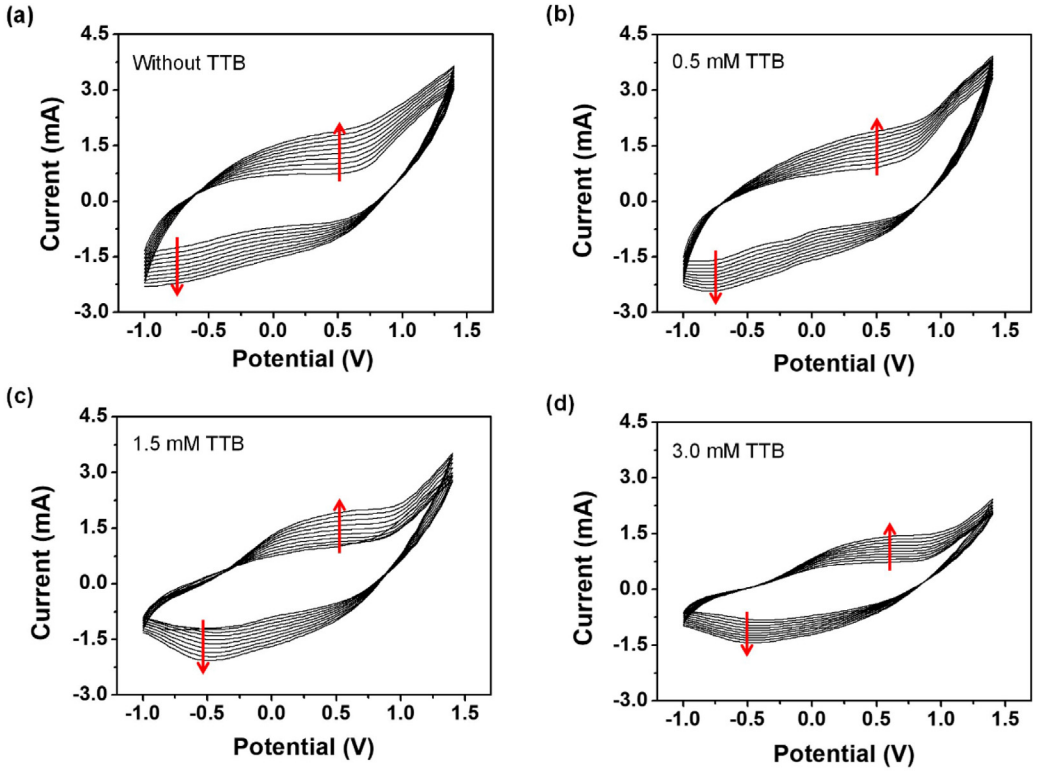

Fig. 2. 10 cycle CV curves of the PEDOT derivatives with different TTB concentration during synthesis: (a), without (PEDOT_0), (b) 0.5 mM (PEDOT_0.5), (c) 1.5 mM (PEDOT_1.5), and (d) 3.0 mM (PEDOT_3.0).

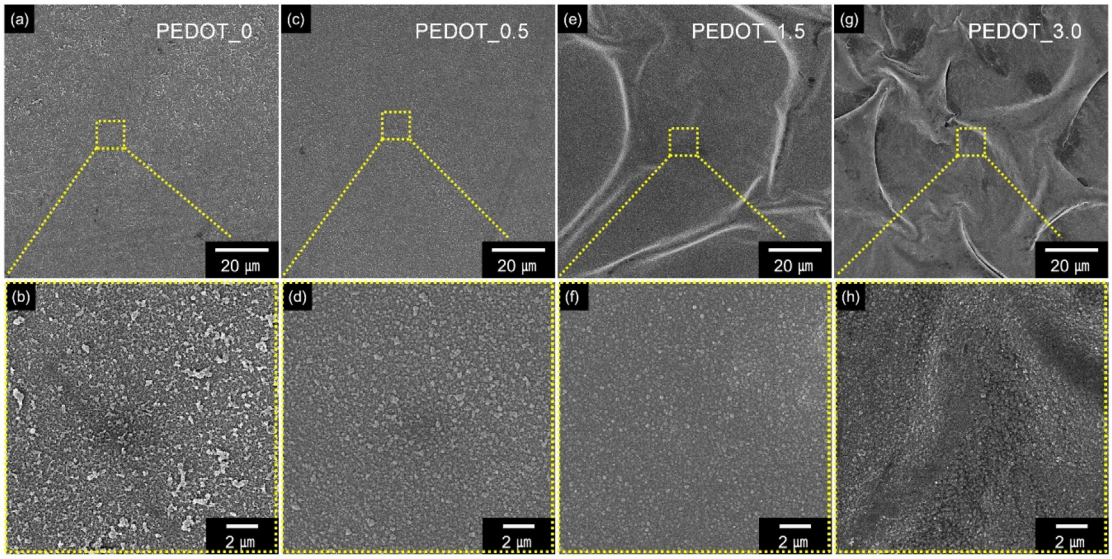

Fig. 3. Low- and high-resolution field-emission scanning electron microscopy (FE-SEM) images of the PEDOT derivative films with different TTB concentrations: (a), (b) PEDOT_0; (c), (d) PEDOT_0.5; (e), (f) PEDOT_1.5; (h), (i) PEDOT_3.0.

(−1 to +1.4) V was selected, because it has the oxidation potential of each monomer (+0.8 V for TTB, and +1.25 V for EDOT).

Fig. 2 and Fig. S2 show CV curves of the different polymerized solutions for a consecutive scan of 10 cycles at a scan rate of 100 mV s^{-1}. The integrated area under the CV curve increases after each cycle, confirming the formation of electroactive polymer films on the ITO substrate. Typically, the CV curves of the only EDOT solution display a wide capacitive response because of overlapping redox peaks (Fig. 2a). On the other hand, the CV curves of the only TTB solution present much smaller current response than the only EDOT solution (Fig. S2). Except for redox peaks at (+0.8 and +0.2) V, there are no significant peaks in the only TTB solution within the scan range. In the mixed monomer solutions, the CV curves are changed with different amount of TTB addition. At 0.5 mM TTB-contained solution, the area of CV curves is larger than that of only EDOT solution (Fig. 2b). The synthesized film has higher electroactivity than the only EDOT solution, despite the TTB addition. In other words, EDOT and TTB form different polymer chain structure from only EDOT and TTB monomers. However, more than 0.5 mM TTB solutions show overall decrease of a current response after each cycle, although they display a similar curve shape (Fig. 2c and d). The decreasing area of CV curves suggests that the less electroactive TTB could be simultaneously polymerized with EDOT, and incorporated into the polymer chain.

The morphology of the polymer film surfaces is significantly changed with the amount of TTB addition. Fig. 3a and b show the bumpy morphology of the pristine PEDOT film (PEDOT_0) with irregular size of grains from (350 nm to 1 μm). Compared to the pristine PEDOT film, the addition of a small amount of TTB (0.5 mM, PEDOT_0.5) transforms to smooth surface with uniform grain size (*ca.* 300 nm), due to TTB being incorporated into the PEDOT chain, and acting as a cross-linking agent (Fig. 3c and d). Furthermore, TTB concentration of higher than 0.5 mM increases the number of buckling patterns with decreasing grain sizes (Fig. 3e–h). In particular, the size of ridges and grains of the films are, respectively, *ca.* 4 μm and *ca.* 250 nm at 1.5 mM of TTB (PEDOT_1.5), and *ca.* 10 μm and *ca.* 200 nm at 3.0 mM of TTB addition (PEDOT_3.0), owing to the excess amount of TTB inducing heterogeneous polymer chains with disturbing the growth of the PEDOT chain, and with polymerizing TTB in the structure. In addition, the change in height according to the addition of TTB of the polymer film was additionally confirmed using the atomic force microscopy (AFM) method (Fig. S3). The introduction of a small amount of TTB into the PEDOT structure significantly reduces the roughness of the polymer surface. However, as the amount of TTB increases, the size of the generated protrusion decreases, but the height change of the film becomes severe, causing wrinkles to fold.

Characterization of PEDOT-derivative films

Raman spectroscopy is used to analyze the structure and bond changes of the polymer chains in each PEDOT derivative, as shown in Fig. 4. The characteristic Raman bands of the polymers share similar features as follows: C—O—C deformation at 1,098 cm^{-1}; C—H in-plane stretching at 1250 cm^{-1}; C—C stretching at 1,370 cm^{-1}; C═C symmetric stretching at *ca.* 1410 cm^{-1}; and C═C asymmetric stretching at 1,535 cm^{-1}. However, the bands about C═C symmetric and C═C asymmetric stretching are changed

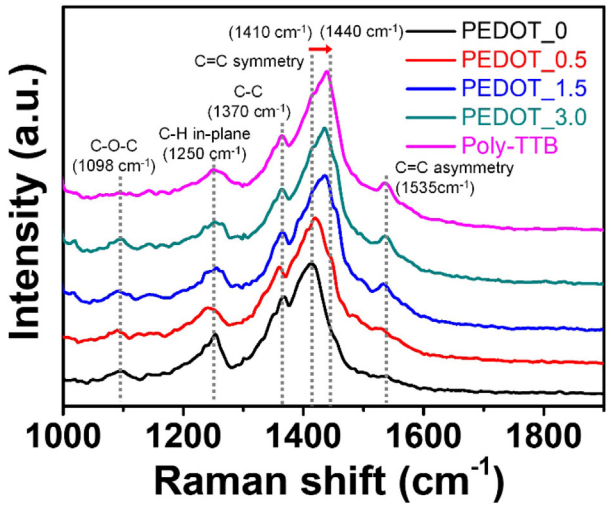

Fig. 4. Raman spectra of the poly-TTB (pink and) the PEDOT derivatives with different TTB concentrations (black: PEDOT_0, red: PEDOT_0.5, blue: PEDOT_1.5, green: PEDOT_3.0).

with different TTB addition amounts. Concretely, the C=C symmetric bands, associated with the structure of graphitic (sp^2) carbon ring, are shifted from 1410 to 1440 cm^{-1} with more TTB addition, owing to the increase in density of the benzene ring in the polymer chain. In contrast, the intensity of the C=C asymmetric band, affiliated with the conjugation length of the polymer chain, increases from more than 0.5 mM of TTB concentration. This data implies that excess amount of TTB reduces the conjugation length of the PEDOT chain with the formation of poly-TTB in the chain structure. Fourier-transform infrared (FT-IR) spectra are also acquired to further characterize the polymer films (Fig. S4). First, the pristine PEDOT (PEDOT_0) film displays several characteristic peaks that are 1535 cm^{-1} for C=C asymmetry, 1410 cm^{-1} for C=C symmetry, 1200 cm^{-1} for C—O stretching, and 1011 cm^{-1} for C—S bending. On the other hand, the peaks for C=C symmetry (1410 cm^{-1}) and for C—H bending of benzene ring at (850 and 730) cm^{-1}, respectively, are shifted, and increase with TTB insertion. In addition, the intensity of the peak for C=C asymmetry (1535 cm^{-1}) is enhanced from 1.5 mM of TTB concentration because of hindrance of the polymerization of EDOT, originating from excess TTB molecule.

The chemical composition of the different polymer films is characterized using X-ray photoelectron spectroscopy (XPS). Fig. 5a shows the C 1s spectra of each polymer film. First, PEDOT_0 reveals several peaks as follows: peaks at (284.7, 285.2, 286.1, 288.0, and 289) eV for C=C and C—C bonds, C—S bond, C—O bonds, carbonyl group, and π–π^* satellite PEDOT chain, respectively [33]. The C 1s spectra at small amount of TTB addition (PEDOT_0.5) suggests similar peaks component distributions, except for reducing the intensity of 286.1 eV (C—O bonds) that originate from EDOT monomer. However, some structural changes are observed in the large amount of TTB contained films (PEDOT_1.5 and PEDOT_3.0). The peak at 288.5 eV (π–π^* satellite of poly-TTB) emerges because polymerized TTB is formed in the PEDOT polymer chain, and the peak of C—O bonds (286.1 eV) also decreases with more TTB molecule inserted into the structure [33]. In addition, the only TTB used polymer film suggests decrease of the peaks-related C—O bonds, and absence of the satellite peak at 289 eV (π–π^* of PEDOT). Moreover, the S 2p region spectra confirm conjugation change of the polymer films with various TTB additions (Fig. 5b). The discrete peaks related to shake-up satellite (*ca.* 169 eV) are improved with increasing the inserted TTB amount. In PEDOT_0 and PEDOT_0.5

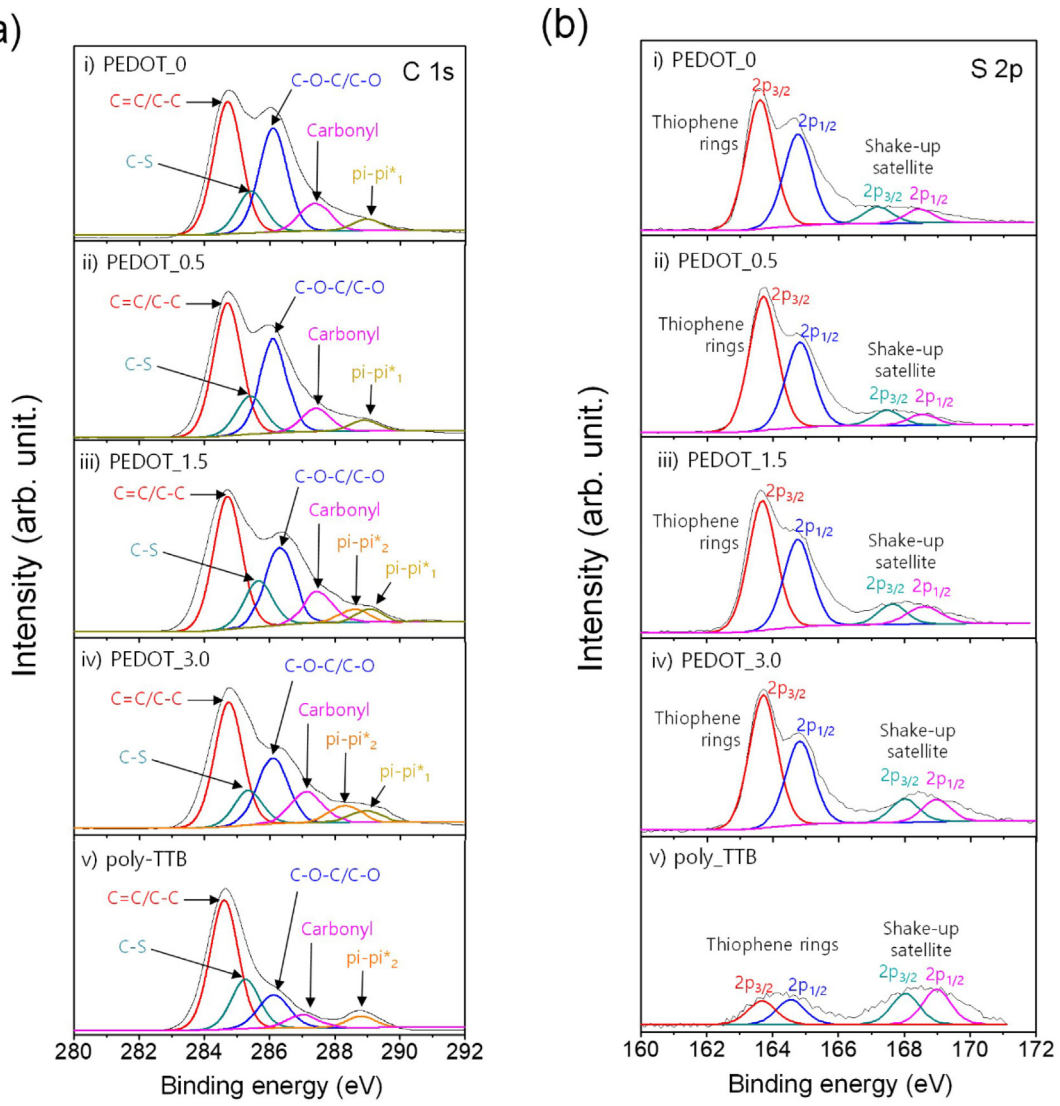

Fig. 5. (a) C 1s and (b) S 2p X-ray photoelectron spectra (XPS) of the different PEDOT and poly-TTB films: (i) PEDOT_0, (ii) PEDOT_0.5 (iii) PEDOT_1.5, (iv) PEDOT_3.0, and (v) poly-TTB.

films, shake-up transitions can occur in the bandgap of the polymer chains. However, more TTB molecules disturb conjugation of the PEDOT chains, then the shake-up transitions that take place during the relaxation generate discrete structures on the high binding-energy side [34].

Optical properties of PEDOT derivative films

The UV–Vis–NIR spectra suggest absorption peaks shifting with different amount of TTB addition. Fig. S5 shows that the PEDOT_0 film displays a low and broad absorption from visible light to the NIR range. On the other hand, only polymerized-TTB (poly-TTB) film represents a high absorption peak around the UV range (*ca.* 300 nm), rather than the visible light and NIR range, owing to poor electron conjugation of the polymer chain (Fig. S6). Therefore, with more TTB inclusion, the absorption peaks of the polymers present move to shorter wavelengths. The absorption peaks of polymers have similar aspects of the PEDOT_0 film until 0.5 mM of TTB addition. However, from 0.75 mM of TTB addition, broad peaks around NIR at (1,000–1,650) nm start to decrease, accompanied by increasing visible light absorption at (400–600) nm. At 1.5 mM of TTB, a new absorption peak of 525 nm is generated with maintaining peaks from (800 to 1,000) nm. In addition, the peak at 525 nm is enhanced until 2.0 mM of TTB. Moreover, at 3.0 mM of TTB addition, the 525 nm absorption peak in the visible light exposes blue shift to 400 nm with improving intensity.

Fig. 6 summarizes the maximum absorption of the polymer films in the different wavelength ranges ((400–600), (800–1000), and 1650) nm. Until 0.5 mM of TTB addition, the maximum absorption peak is similar to that of PEDOT_0 film, which means that after TTB addition, the conjugation length of the polymer chains remains. Therefore, TTB molecules are inserted into the PEDOT without interference of conjugation of the chain structure. However, from 0.75 mM of TTB, the absorption of the 1650 nm is reduced rapidly, while the absorption of the visible light at (400–600) nm increases, on account of the generation of the polymerized TTB structure in the polymer chain. The polymerized TTB structure blocks conjugation of the PEDOT chain, and reduces the doping effect of the polymer [35,36].

Electrochemical properties of the PEDOT-derivative films

The charge transport properties of the PEDOT derivatives are characterized using electrochemical impedance spectroscopy (EIS). The electrochemical test cell was a 3-electrode system composed of Ag/AgCl as the reference electrode, platinum wire as the counter electrode, and polymer-coated platinum wire as the working electrode, in a monomer-free electrolyte solution (Fig. S7). To measure EIS of the polymer films, the bias potential (vs Ag/AgCl) and the scanning frequency were 20 mV, and from (1 MHz to 1 Hz), respectively. Fig. 7a presents the Nyquist plots of the different PEDOT derivative films. The plot of the films shows semi-circle in the high-frequency, and a vertically linear spike in the low-frequency. In particular, the polymer films exhibit different resistive properties in the high-frequency range. The intercept and size of the semi-circle are related to the solution resistance (Rs), and charge transfer resistance at the interface between the electrode and electrolyte (Rct), respectively. The Rs and Rct of the films are reduced by adding a small amount of TTB molecule, as follows: 27.62 Ω (Rs)/227.56 Ω (Rct) for PEDOT_0, and 25.98 Ω (Rs)/159.16 Ω (Rct) for PEDOT_0.5. On the other hand, the values of Rs and Rct of polymer films increase with more TTB addition from 0.5 mM (PEDOT_1.5: 30.75 Ω (Rs)/194.73 Ω (Rct); PEDOT_3.0: 31.64 Ω (Rs)/224.1 Ω (Rct)). In other words, more than 0.5 mM of TTB molecules act as blocking component in the PEDOT chain, due to the Rs and Rct of the poly-TTB being much higher than that of the PEDOT film (Rs = 72.64 Ω, Rct = 4414 Ω) (Fig. S8). Moreover, from 1.5 mM TTB addition, another following semi-circle is generated owing to the polymerization of excess

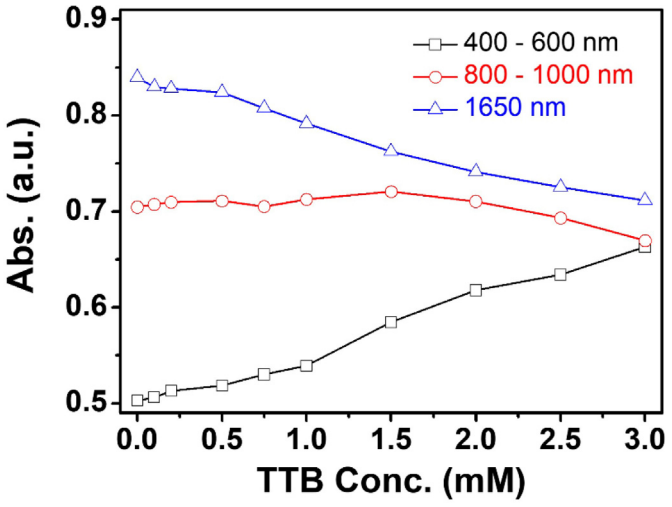

Fig. 6. Normalized absorption of the PEDOT derivatives at the different wavelength ranges: visible (400–600 nm) and near-infrared (800–1000 nm/1650 nm).

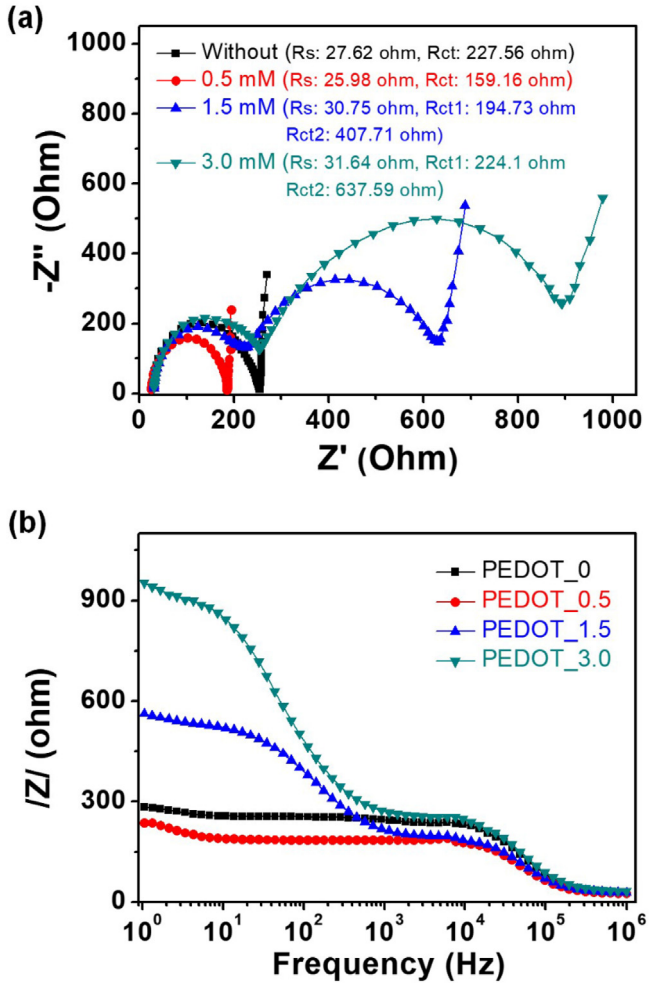

Fig. 7. (a) Nyquist plot and (b) impedance amplitude of the PEDOT derivatives (frequency: 1 MHz to 1 Hz). Black, red, blue, and green represent respectively PEDOT_0, PEDOT_0.5, PEDOT_1.5, and PEDOT_3.0.

TTB molecules in the structure. The diameter of the secondary semi-circle also becomes larger with increasing amount of TTB addition (407.71 and 637.59) Ω for (1.5 and 3.0) mM, respectively. Therefore, excess amount of TTB molecules forms heterogeneous polymer films with the generation of polymerized TTB in the chain structure, and then acts as another source of impedance in the equivalent circuit model (Fig. S9).

Fig. 7b shows the system impedance of the polymer films in the (1 MHz to 1 Hz) frequency range. At high frequency of (10^6–10^4) Hz, the impedance of the polymer films is similar to the increase in value of Rct in the EIS as follow: (227.56, 159.16. 194.73, and 224.1) Ω for PEDOT_0, PEDOT_0.5, PEDOT_1.5, and PEDOT_3.0, respectively. On the other hand, at lower than 10^4 Hz, the impedance is different. For the PEDOT_0 and PEDOT_0.5, the value of the impedance plateaus at constant amount (*ca.* (290 and 250) Ω for PEDOT_0 and PEDOT_0.5, respectively). The impedance of PEDOT_1.5 and PEDOT_3.0 suggests further increase from *ca.* (10^3 to 10^0) Hz because of the second semi-circle originating from the polymerized TTB area. The impedance value of the PEDOT_3.0 film at 100 Hz (*ca.* 950 Ω) is larger than that of the PEDOT_1.5 (*ca.* 570 Ω), due to the increased amount of polymerized TTB in the polymer chain. There are two factors related to the system impedance of the polymer films. For the morphology aspect, smaller grain size with increasing TTB addition causes denser surface of the films, and the intensive polymer surface decreases ion transfer between electrode and electrolyte. From the polymer chain structure, the excess TTB molecules reduce the effective conjugation length of the PEDOT chain because of conduction as a defect to the conjugation backbone.

Crystallinity of the PEDOT-derivative films

The crystallinity of the PEDOT-derivative films was determined using grazing incidence wide-angle X-ray scattering (GIWAXS). The pristine PEDOT (PEDOT_0) film shows weak reflection at 1.7 $Å^{-1}$, associated with π-stacking of the polymer chain, because π-stacking of the PEDOT_0 chains are formed in random direction (Fig. 8a). On the other hand, PEDOT_0.5 film increases the intensity of the reflection (at 1.7 $Å^{-1}$), and displays clearer reflection at out-of-plane direction with the addition of TTB molecule (Fig. 8b). The enhanced reflection implies that the 2D structure of the PEDOT polymer chains generates stable π-stacking perpendicular to the substrate. However, the more than 0.5 mM TTB contained films (PEDOT_1.5 and PEDOT_3.0) display amorphous structure without π-stacking, because polymerized TTB destroys the 2D PEDOT chain structure with copolymerization (Fig. S10). Based on the GIWAXS data, we propose the following schematic of the 2D PEDOT polymer chain packing on the substrate (Fig. 8c). First, the 2D polymer

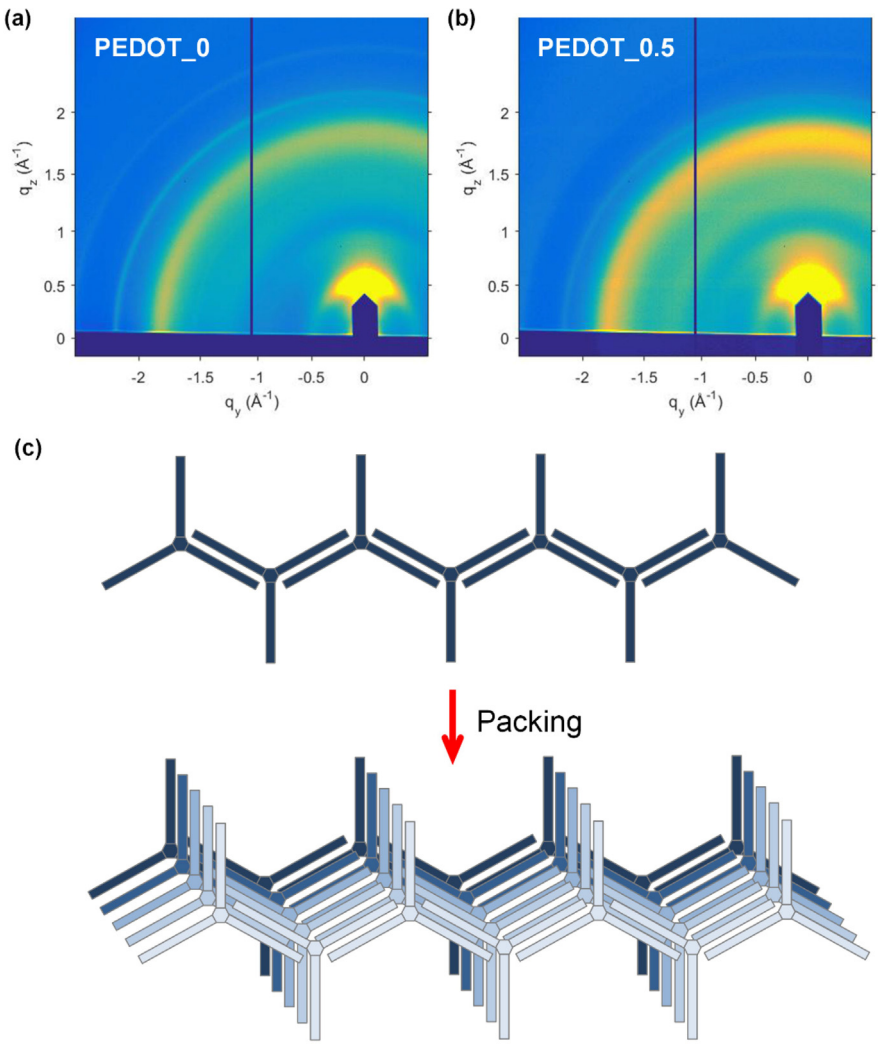

Fig. 8. Grazing incidence wide angle X-ray scattering (GIWAXS) of (a) PEDOT_0 and (b) PEDOT_0.5 films. (c) Scheme of possible three-dimensional packing of star-shaped PEDOT chains.

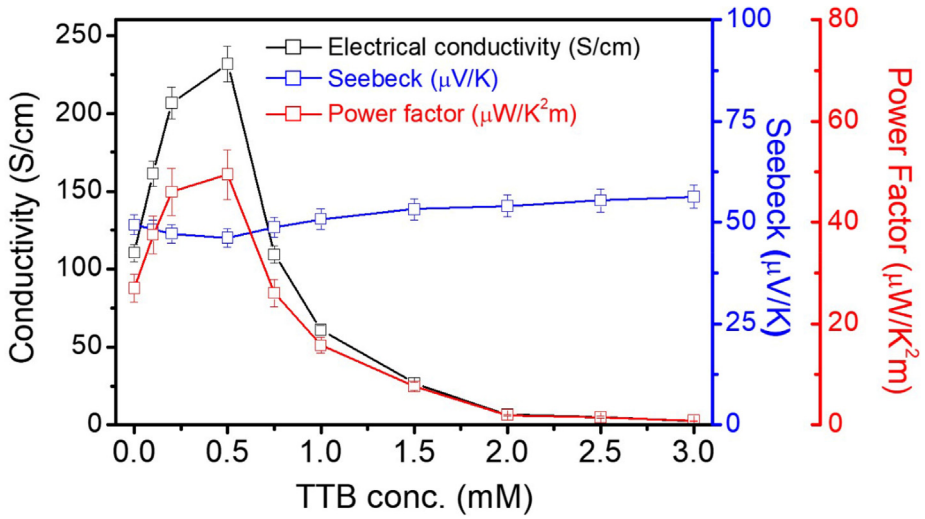

Fig. 9. Thermoelectric properties of the PEDOT derivatives with various TTB concentrations (black: electrical conductivity; blue: Seebeck coefficient; red: power factor).

chains arrange themselves parallel to the surface with the formation of 2D plates. Then, the π–π interactions between 2D PEDOT chains are expected to occur when the chains form π-stacking perpendicular to the surface, which leads to the generation of 3D lamellar structure [37]. The proposed model clearly satisfies the increasing out-of-plane π-stacking of the polymer films.

Performance of the PEDOT-derivative films in thermoelectric application

The substrate used in this work is an ITO-coated PET film. Once the PEDOT-derivative films are grown onto the ITO substrate, the electrical conductivity of the polymer films is higher than that of the original value. To solve this problem, successful transfer of the polymer films from conductive substrate (ITO/PET) to insulating substrate (glass) was performed using adhesive polymer (epoxy resin) (Fig. S11) [38]. The first step was encasing the polymer film in an insulating epoxy adhesive to attach multilayer (epoxy/polymer film/ITP-PET) to a glass surface (second substrate). In particular, the specific epoxy adhesive (Epoxies, No. 20-3302) that had a low thermal expansion coefficient, and could be cured at room temperature (RT), was used to protect crack formation during the thermal curing process. The ITO-PET film (first substrate) peeled away from the polymer surface, resulted in the formation of another multilayer (polymer/epoxy/glass). Then, the transferred polymer films were patterned through gold evaporation to measure the thermoelectric power factor parameters (electrical conductivity (σ), and Seebeck coefficient (S)).

The electrical conductivity according to the change in the oxidation state of the PEDOT derivative films was modified using an electrochemical method. As illustrated in Fig. S12, all polymer films have a highest value of electrical conductivity at 0.6 V as the degree of oxidation increases as the applied voltage increases. Therefore, the thermoelectric performance factor was measured after maintaining the highest electrical conductivity by applying a constant voltage of 0.6 V to the polymer film. To evaluate the thermoelectric properties, four-probe in-plane σ and S measurements were performed on the polymer films at RT. Fig. 9 displays the values of σ, S, and power factor of the films with various TTB concentrations of from (0 to 3.0) mM. The σ and S values of the PEDOT_0 film are 100.5 S cm^{-1} and 49.4 μV K^{-1}, respectively. Small amount TTB additions increase σ of the films with insignificant reduction in S owing to the better crystallinity of the polymer coming from the 2D structure of the chain. At PEDOT_0.5, the polymer film suggests highest σ of 231.8 S cm^{-1} and S of 46.1 μV K^{-1}. On the other hand, more TTB addition causes rapid decrease of σ, with small improvement of S, due to polymerized TTB interruption of the PEDOT chain. Consequently, the values of σ and S at PEDOT_3.0 are 2.64 S cm^{-1} and 56.3 μV K^{-1}, respectively. The following power factor showed highest at PEDOT_0.5 up to 49.43 μV m^{-1} K^{-2} (Table S1). The PEDOT_0.5 has a lower power factor value than the PEDOT:PSS based films, but has a higher value than other conducting polymer chains (Table 1).

Table 1
Comparison of thermoelectric functions of the various PEDOT derivatives and PEDOT films.

Materials	Electrical conductivity (S cm^{-1})	Seebeck coefficient (μV/K)	Power factor (μW m^{-1}K^{-2})	Reference
PBEDTH[1]	0.11	37.2	0.015	[39]
PEBTE[2]	1.6	14	0.03	[40]
PBTTT[3] (FTS[4] doping)	1000	33	110	[41]
PEDOT:PSS	514	42.7	93.5	[42]
PEDOT:PSS (Ethylene glycol and $ZnCl_2$ treated)	2000	27.5	120	[43]
PEDOT:PSS (Ethylene glycol and hydrazine treated)	1300	49	320	[44]
PEDOT_0	110.5	49.4	27.03	This work
PEDOT_0.5	231.8	46.17	49.43	This work

[1] PBEDTH = Poly(1,6-bis((2,3-dihydrothieno[3,4-b][1,4]dioxin-2-yl)methoxy)hexane).
[2] PEBTE = Poly(4,7-bis(2,3-dihydrothieno[3,4-b][1,4]dioxin-5-yl)benzo[c][1,2,5]thiazole).
[3] PBTTT = Poly(2,5-bis(3-tetradecylthiophen-2-yl)thienoyythiophene).
[4] FTS = (tridecafluoro-1,1,2,2-tetrahydrooctyl)trichlorosilane.

Conclusion

In summary, we synthesized two-dimensional PEDOT (2D_PEDOT) chains using a small amount of three-armed conjugated cross-linker (1,3,5-tri(2-thienyl)-benzene (TTB)). The resulting 2D_PEDOT exhibited increasing electrochemical charge transport without shifting of the UV–Vis absorption, and displayed improving π-stacking of the polymer chains, because TTB molecules caused 2D polymer structure parallel to the substrate. The enhanced crystallinity of the PEDOT chains increased the electrical conductivity of the polymer films of (110.5 and 231.8) S cm^{-1} for PEDOT_0 and PEDOT_0.5, respectively, while maintained similar value of the Seebeck coefficient of (49.4 and 46.17) μV K^{-1} for PEDOT_0 and PEDOT_0.5, respectively, which is associated with the charge carrier density of the polymer. The following power factor of the 2D_PEDOT (49.43 μW m^{-1} K^{-2} for PEDOT_0.5) is higher than that of pristine PEDOT (27.03 μW m^{-1} K^{-2} for PEDOT_0) and copolymers of 3,4-ethylenedioxythiophene (EDOT) and TTB (PEDOT-co-TTB) (0.84 μW m^{-1} K^{-2} for PEDOT_3.0). The results reported here indicate that the 2D_PEDOT polymer films would be suitable for use as an electrode material for flexible devices and the thermoelectric generator.

Declaration of Competing Interest

The authors declare that they have no known competing financial interests or personal relationships that could have appeared to influence the work reported in this paper.

Acknowledgment

This work made use of the shared facilities at the University of Chicago Materials Research Science and Engineering Center, supported by National Science Foundation under award number DMR-2011854. Parts of this work were carried out at the Soft Matter Characterization Facility of the University of Chicago. This research used resources of the Advanced Photon Source, an Office of Science User Facility operated for the U.S. Department of Energy (DOE) by Argonne National Laboratory under Contract No. DE-AC-02- 06CH11357. For J.S. Lee, this work was supported by the National Research Foundation of Korea (NRF) grant funded by the Korea government (MSIT) (No. 2020R1A4A407983711).

Appendix A. Supplementary data

Supplementary data to this article can be found online at https://doi.org/10.1016/j.jiec.2022.10.004.

References

[1] J. Jang, Adv. Polym. Sci. 199 (2006) 189–259, https://doi.org/10.1007/12_075.
[2] A. Karki, G. Cincotti, S. Chen, V. Stanishev, V. Darakchieva, C. Wang, et al., Adv. Mater. 34 (2022) 2107172, https://doi.org/10.1002/adma.202107172.
[3] R. Green, M.R. Abidian, Adv. Mater. 27 (2015) 7620–7637, https://doi.org/10.1002/adma.201501810.
[4] T.G. Yun, J. Bae, H.G. Nam, D. Kim, K.R. Yoon, S.M. Han, et al., Nano Energy 94 (2022), https://doi.org/10.1016/j.nanoen.2022.106946.
[5] W. Liu, Z. Lei, R. Yang, W. Xing, P. Tao, W. Shang, et al., ACS Appl. Mater. Interfaces 14 (2022) 10605–10615, https://doi.org/10.1021/acsami.1c19397.
[6] A.M. Glaudell, J.E. Cochran, S.N. Patel, M.L. Chabinyc, Adv. Energy. Mater. 5 (2015) 1401072, https://doi.org/10.1002/aenm.201401072.
[7] B. Russ, A. Glaudell, J.J. Urban, M.L. Chabinyc, R.A. Segalman, Nat. Rev. Mater. 1 (2016) 16050, https://doi.org/10.1038/natrevmats.2016.50.
[8] K. Xu, T.-P. Ruoko, M. Shokrani, D. Scheunemann, H. Abdalla, H. Sun, et al., Adv. Funct. Mater. 32 (2022) 2112276, https://doi.org/10.1002/adfm.202112276.
[9] P.L. Taylor, Phys. L. Rev. B 7 (1973) 1197–1198, https://doi.org/10.1103/PhysRevB. 7.1197.
[10] M. Rastegaralam, M. Rastegaralam, J. Phys. Chem. B 125 (2021) 9910–9915, https://doi.org/10.1021/acs.jpcb.1c06222.
[11] A.T. Ramu, P. Mages, C. Zhang, J.T. Imamura, J.E. Bowers, Rev. Sci. Instrum. 83 (2012), https://doi.org/10.1063/1.4754714.
[12] H. Yan, N. Sada, N. Toshima, J. Therm. Anal. Calorim. 69 (2002) 881–887, https://doi.org/10.1023/a:1020612123826.
[13] F.-X. Jiang, J.-K. Xu, B.-Y. Lu, Y. Xie, R.-J. Huang, L.-F. Li, Chin. Phys. Lett. 25 (2008) 2202, https://doi.org/10.1088/0256-307X/25/6/076.
[14] D. Moses, A. Denenstein, Phys. Rev. B 30 (1984) 2090–2097, https://doi.org/10.1103/PhysRevB.30.2090.
[15] S. Xu, M. Hong, X.-L. Shi, Y. Wang, L. Ge, Y. Bai, et al., Chem. Mater. 31 (2019) 5238–5244, https://doi.org/10.1021/acs.chemmater.9b01500.
[16] S. Perrot, F. Pawula, S. Pechev, G. Hadziioannou, G. Fleury, J. Mater. Chem. C 9 (2021) 7417–7425, https://doi.org/10.1039/D1TC00756D.
[17] J.F. Serrano-Claumarchirant, A.M. Igual-Muñoz, M. Culebras, M.N. Collins, A. Cantarero, C.M. Gómez, Adv. Mater. Interfaces 8 (2021) 2100951, https://doi.org/10.1002/admi.202100951.
[18] S. Horike, Q. Wei, K. Kirihara, M. Mukaida, Y. Koshiba, K. Ishida, J. Mater. Chem. C 9 (2021) 15813–15819, https://doi.org/10.1039/D1TC01385H.
[19] T. Park, C. Park, B. Kim, H. Shin, E. Kim, Energy Environ. Sci. 6 (2013) 788–792, https://doi.org/10.1039/C3EE23729J.
[20] J. Luo, D. Billep, T. Waechtler, T. Otto, M. Toader, O. Gordan, et al., J. Mater. Chem. A 1 (2013) 7576–7583, https://doi.org/10.1039/C3TA11209H.
[21] Z. Fan, J. Ouyang, Adv. Electon. Mater. 5 (2019) 1800769, https://doi.org/10.1002/aelm.20180076.
[22] J. Wang, K. Cai, S. Shen, Org. Electron. physics, Mater. Appl. 17 (2015) 151-158, https://doi.org/10.1016/j.orgel.2014.12.007.
[23] Z.U. Khan, O. Bubnova, M.J. Jafari, R. Brooke, X. Liu, R. Gabrielsson, et al., J. Mater. Chem. C 3 (2015) 10616–10623, https://doi.org/10.1039/C5TC01952D.
[24] B. Kim, C. Cho, M. Han, A.-J. Attias, E. Kim, Adv. Funct. Mater. 31 (2021) 2105297, https://doi.org/10.1002/adfm.202105297.
[25] C. Badre, L. Marquant, A.M. Alsayed, L.A. Hough, Adv. Funct. Mater. 22 (2012) 2723–2727, https://doi.org/10.1002/adfm.201200225.
[26] J. Roncali, P. Leriche, A. Cravino, Adv. Mater. 19 (2007) 2045–2060, https://doi.org/10.1002/adma.200700135.
[27] F. Wang, R.D. Rauh, T.L. Rose, J. Am. Chem. Soc. 119 (1997) 11106–11107, https://doi.org/10.1021/ja970896g.
[28] P.K. Thallapally, K. Chakraborty, H.L. Carrell, S. Kotha, G.R. Desiraju, Tetrahedron 56 (2000) 6721–6728, https://doi.org/10.1016/S0040-4020(00)00493-2.
[29] E. Rebourt, B. Pépin-Donat, E. Dinh, Polymer 36 (1995) 399–412, https://doi.org/10.1016/0032-3861(95)91332-2.
[30] S. Kotha, K. Chakraborty, E. Brahmachary, Syn. Lett. 1999 (1999) 1621–1623, https://doi.org/10.1055/s-1999-2895.
[31] I. Fuks-Janczarek, J.-M. Nunzi, B. Sahraoui, I.V. Kityk, J. Berdowski, A.M. Caminade, et al., Opt. Commun. 209 (2002) 461–466, https://doi.org/10.1016/S0030-4018(02)01686-3.
[32] C. Gu, N. Huang, Y. Chen, L. Qin, H. Xu, S. Zhang, et al., Angew. Chem. Int. Ed. 54 (2015) 13594–13598, https://doi.org/10.1002/anie.201506570.
[33] D.T. Clark, D.B. Adams, A. Dilks, J. Peeling, H.R. Thomas, J. Electron. Spectros. Relat. Phenom. 8 (1976) 51–60, https://doi.org/10.1016/0368-2048(76)80006-0.
[34] G. Morea, L. Sabbatini, R.H. West, J.C. Vickerman, Surf. Interface Anal. 18 (1992) 421–429, https://doi.org/10.1002/sia.740180609.
[35] H.-A. Ho, M. Boissinot, M.G. Bergeron, G. Corbeil, K. Dore, D. Boudreau, et al., Angew. Chem. Int. Ed. 41 (2002) 1548–1551, https://doi.org/10.1002/1521-3773(20020503)41:9<1548::AID-ANIE1548>3.0.CO;2-I.
[36] M. Leclerc, Adv. Mater. 11 (1999) 1491–1498, https://doi.org/10.1002/(SICI)1521-4095(199912)11:18<1491::AID-ADMA1491>3.0.CO;2-O.
[37] S.A. Ponomarenko, S. Kirchmeyer, A. Elschner, B.H. Huisman, A. Karbach, D. Drechsler, Adv. Funct. Mater. 13 (2003) 591–596, https://doi.org/10.1002/adfm.200304363.
[38] M.A. Thomas, J.B. Cui, J. Electrochem. Soc. 160 (2013) D218–D225, https://doi.org/10.1149/2.080306jes.
[39] G. Ye, J. Xu, X. Ma, Q. Zhou, D. Li, Y. Zuo, et al., Electrochim. Acta 224 (2017) 125–132, https://doi.org/10.1016/j.electacta.2016.12.042.
[40] S. Ming, S. Zhen, K. Lin, L. Zhao, J. Xu, B. Lu, et al., J. Electron. Mater. 44 (2015) 1606–1613, https://doi.org/10.1007/s11664-014-3490-x.
[41] S.N. Patel, A.M. Glaudell, D. Kiefer, M.L. Chabinyc, ACS Macro Lett. 5 (2016) 268–272, https://doi.org/10.1021/acsmacrolett.5b00887.
[42] T.A. Yemata, Y. Zheng, A.K.K. Kyaw, X. Wang, J. Song, W.S. Chin, et al., RSC Adv. 10 (2020) 1786–1792, https://doi.org/10.1039/C9RA07648D.
[43] I. Paulraj, T.-F. Liang, T.-S. Yang, C.-H. Wang, J.-L. Chen, Y.-W. Wang, et al., ACS Appl. Energy Mater. 3 (2020) 12447–12459, https://doi.org/10.1021/acsaem.0c02411.
[44] A.G. El-Shamy, Mater. Chem. Phys. 257 (2021) 123762, https://doi.org/10.1016/j.matchemphys.2020.123762.